Γ-*X* mixing in phosphorus-doped silicon nanocrystals: Improvement of photon generation efficiency

Vladimir A. Belyakov and Vladimir A. Burdov
Department of Theoretical Physics, University of Nizhniy Novgorod, Nizhniy Novgorod 603950, Russia
(Received 10 November 2008; revised manuscript received 5 December 2008; published 5 January 2009)

It has been shown theoretically that the central-cell potential of phosphorus ion(s) embedded in a silicon nanocrystal effectively mixes electronic states of *X* and Γ bands. Such a mixing, enhanced by the quantum confinement effect, straightens the nanocrystal band structure and substantially intensifies interband radiative recombination. We have found that it is possible to manipulate the radiative decay rate by varying phosphorus concentration in the nanocrystal.

DOI: 10.1103/PhysRevB.79.035302 PACS number(s): 78.67.Hc, 73.20.Hb, 78.55.Ap

I. INTRODUCTION

Improvement of luminescent properties of various silicon-based structures remains up to now a challenge for modern optoelectronics. Because of indirect band gap of silicon, light emission turns out to be suppressed or completely forbidden. This drawback is partially overcome in nanocrystals (NCs) due to the Heisenberg uncertainty relations and phonon assistance. Previous calculations[1–4] of phonon-assisted radiative recombination rates τ_R^{-1} in Si crystallites yielded the values varying from 10^5 to 5×10^2 s^{-1} as the crystallite radius increases from 1 to 2.5 nm. Recently, Sykora *et al.*[5] reported on the measurements of the decay rates τ_R^{-1} equal to 10^7 s^{-1} but for too small NCs, whose sizes were less, presumably, than 2 nm. At the same time, calculated rate values τ_{NR}^{-1} of the main competitive nonradiative processes, such as capture on dangling bonds or Auger recombination, considerably exceed τ_R^{-1}. For instance, the Auger recombination rates for 2–5 nm crystallites are of the order of 10^7 s^{-1} or greater.[6,7] On average, the rate increases as the NC size decreases. On the contrary, capture on dangling bonds becomes faster in greater NCs. Corresponding rates sharply raise from $\sim10^1$ to 10^{11} s^{-1} for electrons and from 10^7 to 10^{11} s^{-1} for holes (p. 223 of Ref. 8). As a result, interband transitions in silicon NCs should mainly occur through the nonradiative channel. This essentially reduces the quantum yield of the photoluminescence (PL) $\eta=\tau_R^{-1}/\tau_{PL}^{-1}$ in silicon NCs. Here, we introduced the PL rate $\tau_{PL}^{-1}=\tau_R^{-1}+\tau_{NR}^{-1}$. Obviously, if $\tau_R^{-1}\ll\tau_{NR}^{-1}$, total PL time coincides with the smallest time being the time of the nonradiative processes $\tau_{PL}\simeq\tau_{NR}$. Correspondingly, the quantum yield may be written approximately as $\eta=\tau_R^{-1}/\tau_{NR}^{-1}$, which is much less than unity for the above-mentioned typical values of τ_R and τ_{NR}.

However measurements carried out by various experimental groups (see, e.g., Refs 9–13) exhibit τ_{PL} which are not so small as predicted by the theory. Typical values of τ_{PL} vary within a wide range of about 1–1000 μs depending on the particle size, temperature, detected wavelength, method of preparation, etc. Moreover, Miura *et al.*[14] measured τ_R and τ_{NR} separately and found them to be close to each other for different samples containing Si crystallites with different mean diameter varying from sample to sample from 3.5 to 6 nm. They estimated the quantum efficiency as very high and equal to several tenths of percent. That may be possible due to a low excitation power significantly reducing an efficiency of the Auger recombination, and presumably, lower values of the capture rates than that predicted theoretically.[8] This circumstance is an evidence in favor of possible achievement of relatively high values of the quantum yield and PL intensity in real silicon structures. Nevertheless, more often, the PL quantum yield in silicon NCs does not exceed several percent.[15,16] As a consequence, improvement of the PL quantum efficiency in Si NCs remains an actual problem of nanophotonics.

As a means to modify the optical properties of silicon crystallites, doping with shallow impurities has been suggested. In particular, experiments reveal multiple rise of the PL intensity in Si quantum dots due to their doping with phosphorus.[17–21] Usually,[17–21] this is attributed to the passivation of dangling bonds (i.e., neutral or charged P_b centers at the surface) by phosphorus, which decreases the nonradiative recombination rate τ_{NR}^{-1}. However, it has been also shown experimentally[21] that PL lifetime varies weakly with increasing P concentration in the NC, while the PL intensity, which is proportional to η, increases significantly. Hence, the radiative recombination rate changes under doping as well. In other words, introduction of phosphorus into the NCs strongly influences not only the nonradiative channel but also the radiative one. The main purpose of our paper is to understand the mechanism for the PL improvement in P-doped silicon quantum dots and explain the role of phosphorus in the increase in τ_R^{-1}.

We shall first demonstrate theoretically that doping can substantially modify the rate of the radiative transitions in Si NCs. In what follows, within the framework of envelope-function approximation, we calculate the radiative lifetimes for two different cases: (1) doping with a single donor placed in an arbitrary position inside the dot and (2) highly and homogeneously doped dot with donor concentration n_D.

Recently, Iori *et al.*[22,23] computed the imaginary part $\varepsilon''(\omega)$ of the dielectric function of Si NC (the diameter was less than 2 nm) doped with a single P atom. However, it is difficult, as a rule, to extract information about the transitions responsible for PL from the dependence $\varepsilon''(\omega)$. Therefore, it seems to be useful to employ the dielectric function for analysis of absorption spectra rather than emission ones.

Considering the PL, we suppose that main contribution to the emission spectrum comes from the basic interband elec-

tron transitions between the ground conduction and valence states. For this reason, in the following, we shall compute the radiative lifetimes for these transitions only.

First, we discuss the structure of the Coulomb donor field in the NC and its contribution to the electronic state formation in the conduction and valence bands. At this stage, we consider the single-band k-p Hamiltonians and do not take interband interaction into account. Such an approach, described in Sec. II, may be referred to as the zero-approximation model or unperturbed system. Interband mixing of X and Γ bands is discussed in Sec. III. Such a mixing becomes possible due to the short-range character of the donor field and leads to a partial straightening of the band structure of Si NC. In turn, the straightening causes an essential increase in the radiative decay rate, calculation of which is presented in Sec. IV. Finally, in conclusion, we argue the perspectives of some other impurities to be "accelerators" of the radiative interband recombination in silicon NCs.

II. UNPERTURBED SYSTEM

When finding the electronic structure of the P-doped dot, both the long-range hydrogenlike V and the short-range W (so-called central-cell field[24]) parts of the Coulomb potential energy have to be included in a single-particle Hamiltonian. The long-range bulklike hydrogenic potential $V_{\mathrm{H}}=-e^2/\varepsilon_s r$, where ε_s is the silicon permittivity, is transformed in the NC into the sum $V=V_{\mathrm{sp}}(r)+V_{\mathrm{ie}}(\mathbf{r})$ due to appearance of the polarization charges at the NC boundary. Here

$$V_{\mathrm{sp}}(r)=\frac{e^2(\varepsilon_s-\varepsilon_d)}{2\varepsilon_s R}\sum_{l=0}^{\infty}\frac{l+1}{l\varepsilon_s+(l+1)\varepsilon_d}\frac{r^{2l}}{R^{2l}} \tag{1}$$

is the self-polarization potential energy originating from the interaction between the electron and its own image. Here ε_d is the permittivity of the wide-band dielectric matrix surrounding the NC and R stands for the NC radius. The term $V_{\mathrm{ie}}(\mathbf{r})$ describes the direct electron-ion interaction, as well as the interaction of the electron with the ion image,

$$V_{\mathrm{ie}}(\mathbf{r})=-\frac{e^2}{\varepsilon_s|\mathbf{r}-\mathbf{h}|}-\frac{e^2(\varepsilon_s-\varepsilon_d)}{\varepsilon_s R}\sum_{l=0}^{\infty}\frac{h^l r^l}{R^{2l}}\frac{l+1}{l\varepsilon_s+(l+1)\varepsilon_d}P_l(\cos\theta), \tag{2}$$

where $\mathbf{h}$ is the donor position vector, $P_l(\cos\theta)$ is the Legendre polynomial, and θ is the angle between $\mathbf{r}$ and $\mathbf{h}$.

The microscopic short-range part W of the Coulomb potential energy, created by a point charge, is usually constructed with the use of a microscopic dielectric function.[25] We shall employ the dielectric function of Walter and Cohen[26] that can be fitted with the following function:

$$\frac{1}{\varepsilon(k)}=\frac{1}{\varepsilon_s}+\frac{Ak^2}{\alpha^2+k^2}+\frac{(1-A-1/\varepsilon_s)k^2}{\beta^2+k^2}. \tag{3}$$

Here, α and β are equal to 0.82 and 5.0 of the reciprocal Bohr radius, respectively, and $A=1.142$. Pantelides and Sah[25] obtained a resembling expression earlier using a fitting of $1/\varepsilon(k)$ to the data of Nara[27] obtained within the framework of free-electron model. However, $\varepsilon(k)$ dependence found in Ref. 27 turns out to be incorrect at k less than or of the order of $2\pi/a$, where a is the lattice constant of silicon. Meanwhile, precisely the behavior of $\varepsilon(k)$ at small k determines the spatial decay of potential W. More accurate pseudopotential-based calculations of Walter and Cohen[26] allow one to correctly describe $\varepsilon(k)$ in this domain. As a result, the short-range potential is written as follows:

$$W(\mathbf{r},\mathbf{h})=-\frac{e^2}{|\mathbf{r}-\mathbf{h}|}\left[A\exp(-\alpha|\mathbf{r}-\mathbf{h}|)+\left(1-A-\frac{1}{\varepsilon_s}\right)\exp(-\beta|\mathbf{r}-\mathbf{h}|)\right]. \tag{4}$$

As was pointed out earlier by Pantelides and Sah,[25] existence of the local short-range field is an inherent property of the isocoric impurity, such as phosphorus or aluminum. All other impurities produce nonlocal and stronger perturbation, the description of which within the kp method is questionable. The PL enhancement discussed in the present paper is exclusively due to the short-range field of phosphorus, as will be shown below.

If the NC is highly doped, each the electron interacts with all the donors inside the NC and with all other electrons emitted from the donors into the NC. Both the long-range interaction with donors and the electron-electron interaction may be described within the framework of mean-field approximation, in which the electron potential energy $V(\mathbf{r})$ is found from the Poisson equation $div[\varepsilon(r)\nabla V(\mathbf{r})]=4\pi e\rho(\mathbf{r})$. Here e is the positive elementary charge, the dielectric function $\varepsilon(r)$ is equal to ε_s inside and to ε_d outside the NC, and $\rho(\mathbf{r})$ is the charge density that is the sum of two parts; $\rho(\mathbf{r})=\rho_i(\mathbf{r})+\rho_e(\mathbf{r})$, where $\rho_i(\mathbf{r})$ and $\rho_e(\mathbf{r})$ are charge densities of the N donor ions and $N-1$ electrons, respectively. Supposing a high and homogeneous doping inside the dot, it is possible to assume $\rho(\mathbf{r})$ to be equal to the charge density of a single uncompensated positive charge e homogeneously distributed over the dot volume $\rho(r)=3e\Theta(R-r)/4\pi R^3$. Solving Poisson equation with $\rho(r)$ yields inside the NC[28] $V(r)=e^2(r^2/R^2-1-2\varepsilon_s/\varepsilon_d)/2\varepsilon_s R$. This expression should be used for the long-range Coulomb field in the many-donor case instead of the sum $V_{\mathrm{sp}}(r)+V_{\mathrm{ie}}(\mathbf{r})$. On the contrary, short-range field W is not described with the Poisson equation because of its microscopic nature. Therefore, it is included separately in the Schrödinger-type equation as the sum of the terms defined by Eq. (4). Finding envelope functions from the Schrödinger-type equation with long-range field $V(r)$ and short-range field $W=\Sigma_j W(\mathbf{r}-\mathbf{h}_j)$ is described in detail in Ref. 28. Below, we employ the results obtained in this work.

Determination of the electronic structure of a P-doped silicon crystallite exhibits a key role of the short-range field in the electron state formation.[28–34] In particular, in the conduction band, the spinless ground state (being sixfold degenerate in an undoped dot) splits due to the short-range field similar to bulk Si into a singlet with the lowest energy, and doublet and triplet groups of states. Such a splitting occurs, in fact, independent of donors' distribution in the dot. The

wave functions ψ_I of the two (if spin is taken into account) ground states, with initial (I) being the ones under the basic radiative transition, have the form[28]

$$|\psi_I\rangle \equiv |\psi_\sigma\rangle = |\sigma\rangle \sum_{X_1,b} \lambda_b(X_1)|X_1\rangle|b\rangle. \quad (5)$$

Here, $|\sigma\rangle = |\uparrow\rangle, |\downarrow\rangle$ stand for "up" and "down" spinors, $\lambda_b(X_1)$ are the expansion coefficients, $|X_1\rangle$ are the Bloch functions of the representation X_1 of X point, and ket vector $|b\rangle$ describes envelope functions of the isotropic zero-order k-p Hamiltonian (see Ref. 28 for details).

The Bloch functions $|X_1\rangle$ are built in accordance with the symmetry of the irreducible representations A_1, E, and T_2 of the tetrahedral group T_d. In particular, $|A_1\rangle \equiv u_A(\mathbf{r})$ describes the singlet state in the bulk silicon, while $|E^{(1,2)}\rangle \equiv u_E^{(1,2)}(\mathbf{r})$ and $|T_2^{(1,2,3)}\rangle \equiv u_T^{(1,2,3)}(\mathbf{r})$ are the doublet and triplet functions, respectively. Function $|A_1\rangle$ has a nonzero value at the donor site, in contrast to the functions $|E^{(1,2)}\rangle$ and $|T_2^{(1,2,3)}\rangle$, which are equal to zero.[24] Hereafter, we shall use the free-electron Bloch functions represented by plane waves.[35] Such a choice is dictated with not only the simplicity of the model compared to, e.g., the pseudopotential approach, but also a better agreement between the experimental data and the computed energy splitting in the conduction band of bulk silicon.

Because functions $|E^{(1,2)}\rangle$ and $|T_2^{(1,2,3)}\rangle$ describe the doublet and triplet, i.e., excited electron states which are not involved into the basic electron-hole transition, we do not adduce here the explicit expressions for these functions and refer the readers to the book by Yu and Cardona[35] (Sec. IID2) for details. On the contrary, the singlet state contributes to the electron-hole recombination. The Bloch function of the singlet has the form

$$|A_1\rangle = 2 \times \frac{\cos(2\pi x/a)\cos(2\pi y/a) + \text{c.p.}}{\sqrt{3}}, \quad (6)$$

where notation c.p. means two terms obtained from the first one by the cyclic permutations of x, y, and z. The origin of coordinates is situated at an atom. Factor 2 in Eq. (6) provides the correct norm of the total wave function ψ_I.

In order to find the electronic states in the dot, we have to solve the single-particle Schrödinger-type equation for the envelope-function vector $|\Phi\rangle$,

$$[H + U(r) + V(\mathbf{r}) + W(\mathbf{r})]|\Phi\rangle = \varepsilon|\Phi\rangle. \quad (7)$$

Here, H is the bulk $\mathbf{k}\cdot\mathbf{p}$ Hamiltonian operator acting in space of the six-dimensional (6D) envelope-function vectors $|\Phi\rangle$, ε is the electron energy, and $U(r)$ is the confining potential equal to infinity outside the NC and zero inside. The components of the 6D vector $|\Phi\rangle$ are slowly varied expansion coefficients $\Phi_j(\mathbf{r})$ of the total wave function in the Bloch-state basis.

Solving equations such as Eq. (7) has been described in detail in Refs. 28 and 36. The method used there was based on a separation of the Hamiltonian matrix on the isotropic H_0 and anisotropic H_A parts. The isotropic part, called here as the Hamiltonian operator of the zeroth approximation, includes the average of the total k-p Hamiltonian operator over angles in $\mathbf{k}$ space and the confining potential. Anisotropic part contains anisotropic elements of the total k-p Hamiltonian operator and the Coulomb perturbation.

Because of the isotropic and diagonal form of the operator $H_0 + U(r)$, it is possible to classify its eigenstates similar to atomic systems using common terminology such as s-, p-, d-type states, etc. Accordingly, one may formally expand the components of the envelope-function vectors over these eigenstates as

$$\Phi_j(\mathbf{r}) = \sum_b B_{jb}|b\rangle, \quad (8)$$

where $|b\rangle$ stands for the s, p, d states, etc., and B_{jb} are the expansion coefficients.

As was shown in Refs. 28 and 36, it is sufficient to keep in expansion (8) only the s and p states to determine the ground-state envelope functions because all the other unperturbed states have too high energies and weakly mix with the lowest states. The s- and p-type functions can be written as

$$|s\rangle \equiv \phi(r) = \sqrt{\frac{\pi}{2R^3}} j_0(\pi r/R), \quad (9)$$

$$|p_n\rangle \equiv \phi_n(\mathbf{r}) = \sqrt{\frac{3}{2\pi R^3}} \frac{j_1(\mu r/R)}{j_0(\mu)} \frac{x_n}{r},$$

where $n = 1, 2, 3$, $j_{0,1}(x)$ are the spherical Bessel functions, and μ is the first root of $j_1(x)$. Thus, we restrict the set of the envelope functions $|b\rangle$ in the sum in Eq. (5) with only the s- and p-type functions [Eq. (9)].

In the case of the central-symmetric donor distribution inside the NC, coefficient $\lambda_s(A_1)$ in Eq. (5) is close to 1, while all the other coefficients are negligibly small. As a result, wave functions of the two initial states can be represented approximately by $|\psi_\sigma\rangle \approx |A_1\rangle|s\rangle|\sigma\rangle$. If the donor position is asymmetric, all the coefficients $\lambda_b(X_1)$ should be taken into account in expansion (5). In this case, the portions of all Bloch and envelope functions are determined numerically.[28]

Finding of the electron states in the valence band is similar to that described above for the conduction band. The only difference is that we have to take into account the spin-orbit interaction in the k-p Hamiltonian operator and write it in the basis of Bloch functions $|\Gamma_{25'}\rangle$ of Γ point. In the valence band, no additional splitting, other than the spin-orbit one, arises until donors' distribution is of spherical symmetry.[37] In this case, the short-range field results only in a shift of the energy levels. The upper energy level in the valence band is fourfold degenerate. Wave functions ψ_F of this quadruplet [final (F) electron states, or equally, initial hole states] are the products of the Luttinger functions $|M\rangle$ of the total angular momentum 3/2 with $M = \pm 1/2, \pm 3/2$ and the s-type envelope function $|\psi_F\rangle \equiv |\psi_M\rangle = |M\rangle|s\rangle$.[37] If the donor position is asymmetric, M is no longer a good quantum number. In this case, the upper quadruplet splits into two doublets whose wave functions have rather cumbrous expressions.[37] We do not cite them here. Nevertheless, it is possible to write them in some general form similar to that for the initial state [Eq. (5)],

$$|\psi_F\rangle = \sum_{\Gamma_{25'},b,\sigma} \lambda_{b\sigma}(\Gamma_{25'})|\Gamma_{25'}\rangle|b\rangle|\sigma\rangle. \quad (10)$$

Coefficients $\lambda_{b\sigma}(\Gamma_{25'})$ have been found earlier.[37]

Spinless irreducible representation $\Gamma_{25'}$ of the Γ point consists of three basic Bloch functions denoted usually as $|YZ\rangle$, $|XZ\rangle$, or $|XY\rangle$. According to the free-electron model[35] these functions are represented as

$$|YZ\rangle = 2[\sin(2\pi x/a)\cos(2\pi y/a)\cos(2\pi z/a) + \cos(2\pi x/a)\sin(2\pi y/a)\sin(2\pi z/a)],$$

$$|XZ\rangle = 2[\sin(2\pi y/a)\cos(2\pi x/a)\cos(2\pi z/a) + \cos(2\pi y/a)\sin(2\pi x/a)\sin(2\pi z/a)],$$

$$|XY\rangle = 2[\sin(2\pi z/a)\cos(2\pi x/a)\cos(2\pi y/a) + \cos(2\pi z/a)\sin(2\pi x/a)\sin(2\pi y/a)]. \quad (11)$$

It is seen that all Bloch functions $|\Gamma_{25'}\rangle$ are equal to zero at the donor site ($x=y=z=0$).

III. Γ-X MIXING BY THE SHORT-RANGE FIELD

It is well known that indirect radiative transitions may occur with phonon assistance. In this case the phonons compensate the momentum deficiency under the transition. The central-cell donor potential acts similarly. Because of the long-range character in momentum space, the central-cell potential can mix the Bloch states of distant points in the Brillouin zone. In particular, the central-cell field mixes three nonequivalent X points in the conduction band of silicon[24]—X-X mixing that is called usually as a valley-orbit interaction.

Similarly, the central-cell potential couples the Bloch states of the X and Γ points (Γ-X mixing). Naturally, the X-X mixing results in essentially stronger energy corrections[28,30,33] compared to those originated from the Γ-X mixing. At the same time, the Γ-X mixing involves the Bloch states $|\Gamma_{15}\rangle$ and $|\Gamma_{2'}\rangle$ in the initial electron states $|\psi_I\rangle$ and the Bloch states $|X_4\rangle$ in $|\psi_F\rangle$, see Fig. 1. The presence of the Bloch states $|\Gamma_{15}\rangle$ and $|\Gamma_{2'}\rangle$, and $|X_4\rangle$ in the modified initial electron and hole states, respectively, transforms the electron-hole indirect transition into partly direct, which can significantly (1–2 orders of magnitude) increase the radiative recombination rate.

Thus, the short-range donor field mixes the initial $|\psi_I\rangle$ or the final $|\psi_F\rangle$ electron states with the so-called intermediate (i) states $|\psi_i^{(I)}\rangle$ or $|\psi_i^{(F)}\rangle$ having Bloch functions $|\Gamma_{15}\rangle$ and $|\Gamma_{2'}\rangle$ or $|X_4\rangle$, respectively. We neglect all the other X and Γ bands with too low or high energies. Taking into account the short-range Coulomb field as a first-order perturbation, one can modify the wave functions of the initial and final electron states as follows:

$$|\Psi_{I,F}\rangle = |\psi_{I,F}\rangle + \sum_i C_{I,F}(i)|\psi_i^{(I,F)}\rangle. \quad (12)$$

Here, $C_{I,F}(i)=\langle\psi_i^{(I,F)}|W|\psi_{I,F}\rangle/(\varepsilon_{I,F}-\varepsilon_i)$ are the amplitude coefficients of the intermediate states arising due to the donor field, with $\varepsilon_{I,F}$ and ε_i being the energies of the initial/final and intermediate states, respectively. For convenience, one can represent wave functions of the intermediate states $|\psi_i^{(I,F)}\rangle$ in the form similar to $|\psi_I\rangle$ or $|\psi_F\rangle$,

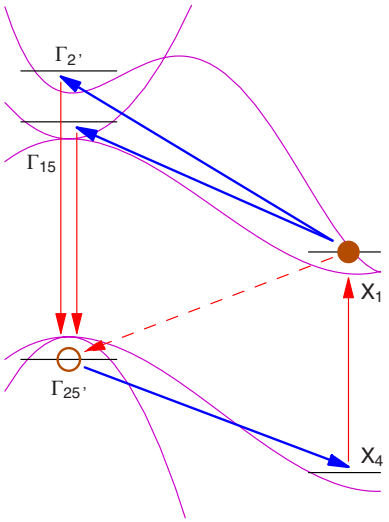

FIG. 1. (Color online) Schematic representation of the phonon-assisted and donor-induced transitions in silicon crystallite. Bold (blue) arrows indicate virtual transitions induced by the donor field or phonon from the initial electron (X_1) and hole ($\Gamma_{25'}$) states to the intermediate states Γ_{15}, $\Gamma_{2'}$, and X_4, respectively. Thin (red) arrows correspond to the transitions with photon from the intermediate states to the final ones. Dashed (red) arrow indicates indirect no-phonon radiative transition between the initial and the final states. Horizontal lines represent energy levels in all the bands involved in the recombination process.

$$|\psi_i^{(I,F)}\rangle = \sum_{\Lambda,b,\sigma} \lambda_{b\sigma}(\Lambda)|\Lambda\rangle|b\rangle|\sigma\rangle, \quad (13)$$

where $|\Lambda\rangle$ are the Bloch functions of representations Γ_{15} and $\Gamma_{2'}$ for $|\psi_i^{(I)}\rangle$ and X_4 for $|\psi_i^{(F)}\rangle$. Expansion coefficients $\lambda_{b\sigma}(\Lambda)$ are determined as solutions of eigenvector and eigenvalue problems for the k-p Hamiltonian operators in Γ_{15}, $\Gamma_{2'}$, and X_4 bands.

Bloch functions $|\Gamma_{15}\rangle$ of triply degenerate band Γ_{15} are usually denoted as $|X\rangle$, $|Y\rangle$, and $|Z\rangle$. From the symmetry point of view, they are similar to the Bloch functions $|YZ\rangle$, $|XZ\rangle$, and $|XY\rangle$ of the band $\Gamma_{25'}$ and differ from them by the sign between the two terms in Eq. (11).[35] $\Gamma_{2'}$ is a simple band described by the Bloch function[35]

$$|\Gamma_{2'}\rangle \equiv |XYZ\rangle = 2[\cos(2\pi x/a)\cos(2\pi y/a)\cos(2\pi z/a) - \sin(2\pi x/a)\sin(2\pi y/a)\sin(2\pi z/a)]. \quad (14)$$

Bloch functions of the sixfold band X_4 may be written as[35] $|X_4^{jk}\rangle = 2\sin(2\pi x_j/a)\cos(2\pi x_k/a)$ with all possible, but differing from each other, values of j and k. For all the above Bloch functions, the coordinates are counted from an atomic site.

In the case where the donor is of substitution type, Bloch functions $|\Gamma_{15}\rangle$ and $|X_4\rangle$ are equal to zero at the donor site while $|\Gamma_{2'}\rangle$ has some finite value. Since the short-range Cou-

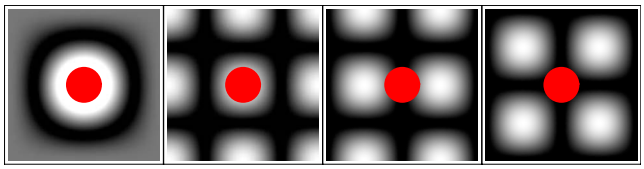

FIG. 2. (Color online) Electron densities in the cross section $z=0$ for the Bloch states $|A_1\rangle$, $|\Gamma_{2'}\rangle$, $|X_4\rangle$, and $|\Gamma_{15}\rangle \equiv |\Gamma_{25'}\rangle$ (from left to right, respectively). White color corresponds to the electron-density maximum, while black color corresponds to zero density. The image size is $a\times a$, where a stands for the lattice constant. The spot in the center represents a lattice site substituted by the donor. The radius of the spot coincides with the typical scale α^{-1} of the short-range potential equal to Bohr radius divided by 0.82 [see Eqs. (3) and (4) in text]. Bloch states $|A_1\rangle$ and $|\Gamma_{2'}\rangle$ have maximal electron density at the donor site in contrast to states $|X_4\rangle$, $|\Gamma_{15}\rangle$, and $|\Gamma_{25'}\rangle$, whose densities are equal to zero.

lomb interaction differs from zero within the nearest vicinity of the donor nucleus, coefficients $C_I(\Gamma_{15})$ and $C_F(X_4)$ have to be much less than $C_I(\Gamma_{2'})$. Figure 2 illustrates this situation. We have depicted in the figure electron densities within a unit cell in plane $z=0$ for the Bloch states $|A_1\rangle$, $|\Gamma_{2'}\rangle$, $|X_4^{12}\rangle$, and $|Z\rangle$ that, in fact, coincides with $-|XY\rangle$ at $z=0$. The donor site is situated at the center of the unit cell and shown with a disk. The disk radius is equal to the typical radius α^{-1} of the short-range donor field. It is seen that the disk covers light areas corresponding to the greatest values of the electron densities in states $|A_1\rangle$ and $|\Gamma_{2'}\rangle$. Therefore, the coupling of Bloch states $|A_1\rangle$ and $|\Gamma_{2'}\rangle$ should be efficient. On the contrary, Bloch states $|\Gamma_{25'}\rangle$, $|\Gamma_{15}\rangle$, and $|X_4\rangle$ have densities close to zero (dark areas) under the disk. This means that mixing of $|A_1\rangle$ with $|\Gamma_{25'}\rangle$ or $|\Gamma_{15}\rangle$, as well as of $|\Gamma_{25'}\rangle$ with $|X_4\rangle$, will be essentially weaker than A_1-$\Gamma_{2'}$ mixing. On this basis, we neglect coefficients $C_I(\Gamma_{15})$ and $C_F(X_4)$ in the subsequent calculations. In turn, $C_I(\Gamma_{2'})$ should be kept in Eq. (12). As a result, the wave function of the final electron state remains invariable, $|\Psi_F\rangle=|\psi_F\rangle$; while the wave function of the initial state is modified by the short-range donor field $|\Psi_I\rangle=|\psi_I\rangle + C_I(\Gamma_{2'})|\psi_{\Gamma_{2'}}\rangle$, where $|\psi_{\Gamma_{2'}}\rangle$ is the wave function in the band $\Gamma_{2'}$.

Since $\Gamma_{2'}$ is a simple band, it is possible to describe electron states in this band with a usual effective-mass approximation as a product of the corresponding Bloch function and some envelope function. In particular, if the donor distribution in the NC has spherical symmetry, the ground state in $\Gamma_{2'}$ band has an envelope function of s type and the total wave function $|\psi_{\Gamma_{2'}}\rangle=|\Gamma_{2'}\rangle|s\rangle$. All the other states in $\Gamma_{2'}$ band have p-, d-, $2s$-type, etc., envelope functions and slightly contribute to the Γ-X mixing. In case of asymmetric donor distribution, the envelope function of the ground state in the $\Gamma_{2'}$ band will be predominantly a result of the s-p hybridization. Then the expression for the wave function of the intermediate state [Eq. (13)] is transformed into $|\psi_{\Gamma_{2'}}\rangle = |\Gamma_{2'}\rangle|\sigma\rangle\Sigma_b\lambda_b(\Gamma_{2'})|b\rangle$, where index b runs over s, p_x, p_y, and p_z.

Consequently, we have to determine the only coefficient $C_I(\Gamma_{2'})=\langle\psi_{\Gamma_{2'}}|W|\psi_I\rangle/[\varepsilon(A_1)-\varepsilon(\Gamma_{2'})]$ for the ground state in $\Gamma_{2'}$ band. Here, $\varepsilon(A_1)$ is the energy of the initial state—the ground state in the X_1 band. In order to calculate the matrix element $\langle\psi_{\Gamma_{2'}}|W|\psi_I\rangle$, we employ Eq. (4) for W and Eqs. (6) and (14) for the Bloch functions. Energies $\varepsilon(A_1)$ and $\varepsilon(\Gamma_{2'})$, as well as expansion coefficients $\lambda_b(\Gamma_{2'})$, can be found analytically at spherically symmetric donor position inside the NC (see, e.g., Ref. 28 for the initial state). Otherwise, the energies and expansion coefficients are determined numerically.

IV. RADIATIVE DECAY RATE

Traditionally, indirect radiative transitions become more extensive if phonons assist recombination. However, we have found that doping with phosphorus can be an alternative and an even more efficient means to intensify the radiative recombination channel.

Let us compute the transition rates between all possible I and F states. Due to the degeneracy of both the initial and final electron states, there are more than one basic transitions $I\rightarrow F$. Therefore, it is possible to introduce the rate $\tau_R^{-1}(I,F)$ for each $I\rightarrow F$ transition, with rate τ_R^{-1} being the average. Obviously, the donor-induced and the phonon-assisted transitions individually contribute to the total decay rate $\tau_R^{-1}(I,F)$ which, hence, may be represented as $\tau_D^{-1}(I,F)+\tau_{\rm ph}^{-1}(I,F)$. In the following, we calculate separately the donor-induced $\tau_D^{-1}(I,F)$ and phonon-assisted $\tau_{\rm ph}^{-1}(I,F)$ decay rates, as well as their averages τ_D^{-1} and $\tau_{\rm ph}^{-1}$.

When calculating $\tau_{\rm ph}^{-1}$, we neglect the Γ-X mixing caused by the short-range field. Such a process weakly influences the phonon-assisted radiative recombination. At the same time, the valley-orbit coupling in the conduction band and the central-cell corrections in the valence band affect the decay rate. These processes transform wave functions $|\psi_I\rangle$ and $|\psi_F\rangle$, and correspondingly, the phonon-assisted recombination rate related to those in undoped dots.

The phonon-assisted radiative decay is the second-order process. It requires a participation of both photon and phonon, as shown schematically in Fig. 1. Phonon mixes the initial electron state having Bloch function $|A_1\rangle$ with the intermediate states having Bloch functions $|\Gamma_{15}\rangle$ and $|\Gamma_{2'}\rangle$. Also, the initial hole state (or, equivalently, the final electron state) having Bloch function $|\Gamma_{25'}\rangle$ mixes with the phonon with the intermediate state $|X_4\rangle$. Our calculations show that the phonon-assisted radiative transition through state $|\Gamma_{2'}\rangle$ is less efficient and weakly contributes to $\tau_{\rm ph}^{-1}(I,F)$ and $\tau_{\rm ph}^{-1}$. Decay rates $\tau_{\rm ph}^{-1}(I,F)$ are calculated with the Fermi golden rule that can be written for the second-order process in the form

$$\tau_{\rm ph}^{-1}(I,F) = \frac{2\pi}{\hbar}\sum_{\mathbf{Q},\alpha}\sum_{\mathbf{q},\ell}\left|\sum_i \frac{U_{Fi}^{(\rm opt)}U_{iI}^{(\rm lat)}+U_{Fi}^{(\rm lat)}U_{iI}^{(\rm opt)}}{E_I-E_i}\right|^2 \times\{\delta[\varepsilon_g(R)-\hbar\omega_\alpha(\mathbf{Q})-\hbar\nu_\ell(\mathbf{q})] + \delta[\varepsilon_g(R)-\hbar\omega_\alpha(\mathbf{Q})+\hbar\nu_\ell(\mathbf{q})]\}. \quad (15)$$

Here, matrix elements of the electron-photon ($U^{(\rm opt)}$) and electron-phonon ($U^{(\rm lat)}$) interaction operators are calculated among the initial I, the final F, and the intermediate state i; E_i and E_I are the total energies of the intermediate and initial

states, respectively, including not only the energies of the electrons (or holes) but also the energies of the photon and phonon reservoirs. The phonon frequency of ℓth mode is denoted as $\nu_\ell(\mathbf{q})$ with $\mathbf{q}$ being the phonon wave vector and the photon frequency of αth polarization is $\omega_\alpha(\mathbf{Q})$, where $\mathbf{Q}$ stands for the photon wave vector. $\varepsilon_g(R)$ is the NC gap depending on the dot radius.

The electron-phonon interaction operator is treated within the framework of the rigid-ion model and is given by

$$U^{(\mathrm{lat})} = -\sum_{\mathbf{q},\ell}\sum_{\mathbf{n},s}\sqrt{\frac{\hbar}{2M_0N_0\nu_\ell(\mathbf{q})}}\nabla V_{\mathbf{n}s}(\mathbf{e}_{\mathbf{q}\ell s}\exp\{i\mathbf{q}\mathbf{R}_\mathbf{n}\}b_{\mathbf{q}\ell} + \mathbf{e}^*_{\mathbf{q}\ell s}\exp\{-i\mathbf{q}\mathbf{R}_\mathbf{n}\}b^+_{\mathbf{q}\ell}). \quad (16)$$

Here, N_0 is the number of primitive cells in the crystal, M_0 is the mass of a silicon atom, $V_{\mathbf{n}s}=V_{\mathrm{at}}(\mathbf{r}-\mathbf{R}_\mathbf{n}-\boldsymbol{\tau}_s)$ is the atomic potential, where $\mathbf{R}_\mathbf{n}$ stands for the position vector of the $\mathbf{n}$th unit cell, and $\boldsymbol{\tau}_s$ represents the position vectors of two atoms within the unit cell, $\boldsymbol{\tau}_1=0$ and $\boldsymbol{\tau}_2=(1,1,1)\times a/4$, $b^+_{\mathbf{q}\ell}$ and $b_{\mathbf{q}\ell}$ are the phonon creation and annihilation operators, and the phonon polarization vectors are denoted as $\mathbf{e}_{\mathbf{q}\ell s}$. Further evaluation of $U^{(\mathrm{lat})}_{il}$ and $U^{(\mathrm{lat})}_{Fi}$ matrix elements is associated with the Fourier transformation of $V_{\mathrm{at}}(\mathbf{r})$ calculated with the pseudopotential method. The similar procedure was applied by Glembocki and Pollak[38,39] for computing electron-phonon matrix elements in bulk silicon.

The electron-photon interaction is described by the operator

$$U^{(\mathrm{opt})} = \sum_{\mathbf{Q},\sigma}\sqrt{\frac{2\pi\hbar e^2\kappa(\varepsilon_s;\varepsilon_d)}{m_0^2\omega_\sigma(\mathbf{Q})V_0\varepsilon_d^{3/2}}}(c_{\mathbf{Q}\sigma}+c^+_{\mathbf{Q}\sigma})\mathbf{e}_{\mathbf{Q}\sigma}\mathbf{p}, \quad (17)$$

where $-e$ and m_0 are free-electron charge and mass, respectively, $\mathbf{p}=-i\hbar\nabla$ is the electron momentum operator, $\mathbf{e}_{\mathbf{Q}\sigma}$ is the photon polarization vector, the operator $c_{\mathbf{Q}\sigma}$ annihilates and $c^+_{\mathbf{Q}\sigma}$ creates a photon with the wave vector $\mathbf{Q}$ and polarization σ, and V_0 stands for the volume of the electromagnetic resonator. Function $\kappa(\varepsilon_s;\varepsilon_d)=9\varepsilon_d^{5/2}/(2\varepsilon_d+\varepsilon_s)^2$ appears due to the replacement of homogeneous media with bulk permittivity ε_s by a spherical silicon nanocrystal surrounded by a dielectric wide-band matrix with a dielectric constant ε_d.[40]

Calculations of the phonon-assisted radiative decay rates in accordance with Eq. (15) and using wave functions of the initial, final, and intermediate states defined by Eqs. (5), (10), and (13), respectively, yield the results presented in Fig. 3. We have plotted in the figure ratio $\tau_{\mathrm{ph}}^{-1}/\tau_0^{-1}$ of the average phonon-assisted decay rates in the doped (τ_{ph}^{-1}) and undoped (τ_0^{-1}) NCs. As one can see, the phonon-assisted recombination in the P-doped dot is always slower than that in the undoped one (dashed lines in Figs. 3 and 4), except for the case of the central-located donor in the NCs greater than 2 nm in radius. Nevertheless, even in this case, the decay-rate increase does not exceed 1%–2%. In turn, maximal decrease in the decay rate (about 50%) corresponds to the donor displacement from the dot center h close to $R/2$. This is easy to explain by the weakest overlap of the electron wave functions of the initial and final states. Doping with high donor concentration $n_D=2\%$ (2 P atom per 98 Si atoms, which

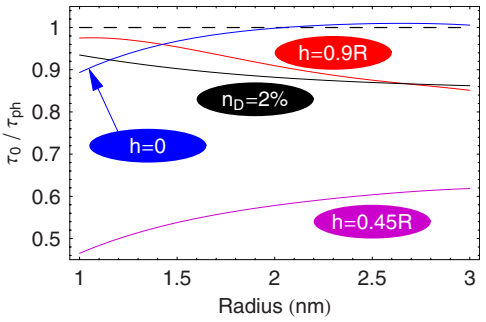

FIG. 3. (Color online) Ratio of the average phonon-assisted decay rates in the doped and undoped dots as a function of the dot size. Dashed line: $\tau_{\mathrm{ph}}^{-1}=\tau_0^{-1}$. Donor displacement h relative to the dot center if the dot is single doped and the donor concentration, in the case of homogeneously doped dot, is indicated in the figure.

corresponds to the phosphorus concentration 1 nm^{-3}) is also inefficient for the phonon-assisted radiative transitions—the decay rate becomes 5%–15% less. Evidently, doping cannot improve the phonon-assisted photon generation in silicon crystallites.

Let us now consider the no-phonon radiative transitions induced by the short-range donor field in quantum dots and compute donor-induced transition rates $\tau_D^{-1}(I,F)$ between all possible I and F states, and average rate τ_D^{-1}. In order to compute the rates we employ the Fermi golden rule for the first-order process. After some algebra, one can obtain

$$\tau_D^{-1}(I,F) = \frac{4e^2\kappa(\varepsilon_s;\varepsilon_d)\varepsilon_g(R)}{3m_0^2\hbar^2c^3}|\mathbf{p}_{IF}|^2. \quad (18)$$

Here, c stands for the vacuum speed of light and $\mathbf{p}_{IF}=\langle\Psi_I|\mathbf{p}|\Psi_F\rangle$. It is important to emphasize, however, that the wave functions of the initial states in $\mathbf{p}_{IF}$ are transformed into $|\Psi_I\rangle=|\psi_I\rangle+C_I(\Gamma_{2'})|\psi_{\Gamma_{2'}}\rangle$, while the wave functions of the final states remain invariable $|\Psi_F\rangle=|\psi_F\rangle$ (see Sec. III).

Thus [Eq. (18)], the rate of the no-phonon radiative transitions induced by the short-range donor field is defined by a squared magnitude of $|\mathbf{p}_{IF}|\equiv p_{IF}=p_{\mathrm{cv}}|C_I(\Gamma_{2'})|$. Here, p_{cv} is the so-called momentum matrix element arising usually in

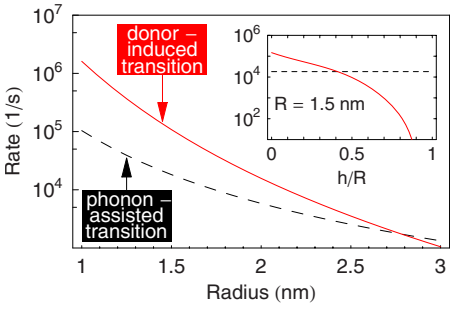

FIG. 4. (Color online) Average rates of the donor-induced (solid line) and the phonon-assisted (dashed line) radiative transitions vs the dot size for the single-doped dot. The phosphorus ion is located at the dot center ($h=0$). Inset: decay rate τ_D^{-1} as a function of the dimensionless donor displacement from the dot center—solid line. Horizontal dashed line represents τ_0^{-1}.

the Fermi golden rule for direct electron transitions. In the frames of the free-electron model $p_{cv}=2\pi\hbar/a$. For indirect transitions in silicon crystallites, optical matrix element p_{IF} acquires additional small factor $C_I(\Gamma_{2'})$ close to 0.1 for 2–3 nm crystallites and decreasing as the NC size increases. In what follows, we shall find $C_I(\Gamma_{2'})$ and calculate $\tau_D^{-1}(I,F)$ and τ_D^{-1} for many- and single-donor cases.

Figure 4 presents a dependence of the decay rates on the dot radius for the single-donor case when the phosphorus ion occupies the dot center. If the phosphorus distribution in the dot is of spherical symmetry, the initial and final electron states may be symbolically labeled as σ and M, and the rates may be denoted as $\tau_D^{-1}(\sigma,M)$. In this case it is possible to show that six of the eight electron transitions are allowed, and their rates obey the following equalities: $\tau_D^{-1}(\uparrow,3/2)=\tau_D^{-1}(\downarrow,-3/2)\equiv 2\tau_D^{-1}$, $\tau_D^{-1}(\uparrow,1/2)=\tau_D^{-1}(\downarrow,-1/2)\equiv 4\tau_D^{-1}/3$, and $\tau_D^{-1}(\uparrow,-1/2)=\tau_D^{-1}(\downarrow,1/2)\equiv 2\tau_D^{-1}/3$. The two residual transitions ($|\uparrow\rangle\rightarrow|-3/2\rangle$ and $|\downarrow\rangle\rightarrow|3/2\rangle$) are spin forbidden. Average decay rate τ_D^{-1} is depicted in the figure. One can see that in a wide range of the dot sizes, the donor-induced radiative transitions turn out to be faster than the phonon-assisted transitions in undoped NCs, whose average rate τ_0^{-1} is shown with a dashed line. This trend is more pronounced for smaller sizes, e.g., at $R=1$ nm, τ_D^{-1} exceeds τ_0^{-1} by more than an order of magnitude. It is a consequence of the quantum confinement effect. Due to the short-range character of field W, matrix element $\langle\psi_{\Gamma_{2'}}|W|\psi_\sigma\rangle$ is, in fact, proportional to the squared value of s-type envelope function $\phi^2(0)$. According to Eq. (9), it means that $\langle\psi_{\Gamma_{2'}}|W|\psi_\sigma\rangle\sim R^{-3}$ and $\tau_D^{-1}(\sigma,M)\sim R^{-6}$ and sharply rises as the NC size decreases.

However, such a relationship between τ_D^{-1} and τ_0^{-1} turns into the opposite one if the donor shifts toward the NC surface, see inset of Fig. 4. Beyond half the dot radius, average decay rate τ_D^{-1} drops with increasing h. The origin of this sharp decrease lies in a strong weakening of the central-cell interaction near the dot boundary and the wave-function reconstruction leading to a certain spatial separation of the electron densities in the conduction and valence bands. In particular, electron density in the conduction band tends to accumulate near the donor, while the valence-band density tends to occupy donor-free areas. Thus, the donor-induced radiative recombination substantially decelerates as the system asymmetry rises.

In the case of high and homogeneous doping, the system completely restores its spherical symmetry. Moreover, the spatial separation of the charge densities in different bands becomes impossible because no areas, which would be free of donors, exist in the NC. As a result, at donor concentrations n_D greater than approximately 1% (1 P atom per 99 Si atoms), we find the average rates τ_D^{-1} to be much greater than τ_0^{-1} for all dot sizes, see Fig. 5. At $n_D=0$, τ_D turns into infinity, and the total decay rate τ_R^{-1} is equal to τ_0^{-1} (lowest curve in Fig. 5). Increasing phosphorus concentration leads to a sharp rise of τ_D^{-1} with respect to τ_0^{-1}, especially for bigger crystallites, as is seen in Fig. 6. For instance, at $n_D=2\%$, τ_D^{-1} becomes 1–2.5 orders of magnitude greater than τ_0^{-1} as the dot radius increases from 1 to 3 nm, respectively.

The increase in τ_D^{-1} in the many-donor case is quite understandable based on the behavior $\tau_D^{-1}(h)$ in the single-donor

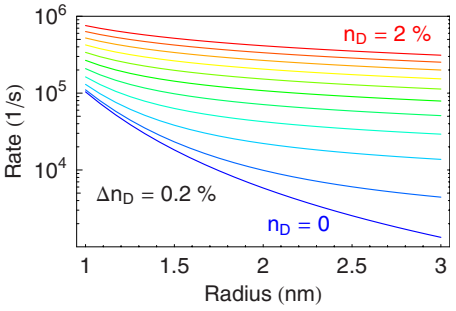

FIG. 5. (Color online) Total average recombination rate $\tau_R^{-1}=\tau_D^{-1}+\tau_{\rm ph}^{-1}$ as a function of the dot radius at donor concentration n_D increasing with the constant step of 0.2% from 0 to 2%.

case. As shown in the inset of Fig. 4, the main contribution to the acceleration of the donor-induced transitions comes from the donors situated near the dot center. Increasing n_D results in an accumulation of the greater amount of donors around the dot center. This increases the number of channels for the donor-induced transitions, which shorten the time τ_D. As a result, increase in the total rate τ_R^{-1} turns out to be the same. Obviously, from the viewpoint of photon generation, Γ-X mixing due to the short-range field is more efficient than the phonon assistance. The obtained values of the donor-induced recombination rates are already comparable with typical values of the capture rates on dangling bonds (p. 223 of Ref. 8), especially for smaller crystallites.

The dependence τ_D^{-1} on the donor concentration is an important feature of the donor-induced radiative recombination in the many-donor case. This dependence appears in the recombination rate because of its proportionality to the squared absolute value of $\langle\psi_{\Gamma_{2'}}|W|\psi_I\rangle$ [$|\mathbf{p}_{IF}|^2$ in Eq. (18)]. In the many-donor case, the short-range potential turns into the sum

$$W=\sum_{j=1}^{N} W(\mathbf{r},\mathbf{h}_j), \tag{19}$$

where N is the number of donors in the NC and $W(\mathbf{r},\mathbf{h}_j)$ stands for the single-donor field described by Eq. (4). Assuming the donor distribution to be of spherical symmetry, one can set $|\psi_I\rangle=|A_1\rangle|s\rangle$, $|\psi_{\Gamma_{2'}}\rangle=|\Gamma_{2'}\rangle|s\rangle$, and write the matrix

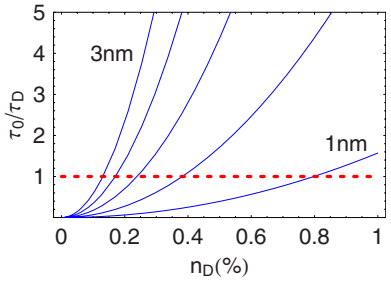

FIG. 6. (Color online) Relative rate τ_0/τ_D as a function of the phosphorus concentration for radius R increasing with the constant step of 0.5 nm from 1 to 3 nm (from right to left).

element $\langle\psi_{\Gamma_{2'}}|W|\psi_I\rangle$ as integral $\int W\phi^2(r)u_\Gamma^*(\mathbf{r})u_A(\mathbf{r})dV$, where $u_\Gamma(\mathbf{r})\equiv|\Gamma_{2'}\rangle$ and $u_A(\mathbf{r})\equiv|A_1\rangle$. Envelope function $\phi(r)$ varies on a scale of the NC size (2–6 nm), while $W(\mathbf{r},\mathbf{h}_j)$ differs from zero within 1–2 Bohr radii ($\sim$1 Å) around the donor nucleus. Accordingly, when integrating $\phi^2(r)$ multiplied by $W(\mathbf{r},\mathbf{h}_j)$, we may take $\phi(r)$ as a constant equal to $\phi(h_j)$. Then, using Eqs. (6) and (14) for the Bloch functions of A_1 and $\Gamma_{2'}$ bands, respectively, and the explicit expression for the short-range potential [Eq. (4)], one can obtain the matrix element in the form

$$\langle\psi_{\Gamma_{2'}}|W|\psi_I\rangle = -4\pi\sqrt{3}[Ag(\alpha)-(A+1/\varepsilon_s-1)g(\beta)]e^2N\langle\phi^2\rangle_N,$$

where $\langle\phi^2\rangle_N=N^{-1}\Sigma_j\phi^2(h_j)$ and

$$g(x)=(x^2+4\pi^2/a^2)^{-1}+2(x^2+20\pi^2/a^2)^{-1}+(x^2+36\pi^2/a^2)^{-1}.$$

Because $\alpha\ll\beta$, the term $(A+1/\varepsilon_s-1)g(\beta)$ is negligibly small compared to $Ag(\alpha)$. Finally, supposing the homogeneous donor distribution in the NC, we replace the average over the number of donors $\langle\phi^2\rangle_N$ by the average over the NC volume $\langle\phi^2\rangle_V=V^{-1}\int\phi^2(h)d^3h$, which equals V^{-1} due to normalization condition for the envelope functions. This yields

$$\langle\psi_{\Gamma_{2'}}|W|\psi_I\rangle = -4\pi\sqrt{3}Ag(\alpha)e^2n_D, \tag{20}$$

where the average donor concentration n_D has been introduced as N/V.

Thus, by varying n_D it is possible to manipulate the radiative channel efficiency. Since, according to Eq. (20), $\langle\psi_{\Gamma_{2'}}|W|\psi_I\rangle\sim n_D$, dependence $\tau_D^{-1}(n_D)$ is close to quadratic, as shown in Fig. 6 for five different values of the dot radius. Bearing in mind the proportionality of the PL intensity to τ_R^{-1} and taking into account that $\tau_R^{-1}\approx\tau_D^{-1}$ at n_D greater than $\sim$1%, one may conclude that $I_{\mathrm{PL}}\sim n_D^2$. However, the experimentally observed dependence $I_{\mathrm{PL}}(n_D)$ is rather logarithmic or rooted.[20,21] As a result, the observed enhancement of the PL intensity with increasing phosphorus concentration is not so large, as one could expect from an increase in the decay rate shown in Fig. 5. Perhaps, some other factors, except for the decay rate, can influence I_{PL}. In particular, the PL intensity is directly proportional to the photon absorption cross section σ_0. Dependence $\sigma_0(n_D)$ is unknown; therefore, an exact description of the function $I_{\mathrm{PL}}(n_D)$ is not a simple task.

Nevertheless, the main statement, following from our study, is that phosphorus doping influences not only the nonradiative channel of the interband recombination in silicon crystallites but also the radiative channel. The performed theoretical analysis exhibits a possibility of the substantial decrease in the radiative lifetime τ_R due to the short-range Coulomb field of a phosphorus ion. In turn, this improves the photon generation efficiency in silicon crystallites.

V. CONCLUSION

In this paper, we have considered only phosphorus as a dopant. As was mentioned above, all the other donors of group V, as well as the group III acceptors, except B and Al, create short-range field that is more complicated compared to the point-charge field [Eq. (4)]. Correct description of these fields requires an application of the first-principles methods, which go beyond the frames of our study. Therefore, we did not touch upon the problem of radiative recombination in silicon NCs with various impurities of groups III and V. With respect to boron and aluminum, it is possible to make some conclusions related to their influence on the radiative decay in Si NCs.

According to the calculations of Lipari and Baldereschi,[41] boron may be treated, presumably, as a hydrogenlike acceptor that does not create the short-range field. On this reason, efficient Γ-X mixing and the band-structure straightening in silicon quantum dots are impossible under B doping. Such conclusion is corroborated both theoretically[4] and experimentally.[42]

On the contrary, aluminum is an isocoric impurity for silicon as well as phosphorus. Consequently, aluminum ion produces the short-range field of the point-charge type similar to that produced by the phosphorus ion [Eq. (4)]. The only difference is that the short-range potential of the aluminum ion will be of the opposite sign with respect to the one written in Eq. (4). This circumstance plays a crucial role in the electronic structure formation in Si NC doped with aluminum. In this case, the valley-orbit interaction splits the sixfold-degenerate ground state in the conduction band into the singlet, doublet, and triplet as before. However, the singlet level splits off upward because of the repelling character of the short-range field of aluminum ion in contrast to the attracting character of the phosphorus-ion field. At the same time, independent of the impurity type, the valley-orbit interaction weakly influences the doublet and triplet levels. As a result, the ground state in the Al-doped dot will be of the doublet or triplet type, while the singlet state will be strongly excited. In turn, the doublet or triplet states have $|E\rangle$ or $|T_2\rangle$ Bloch functions, respectively, which slightly mix with the intermediate states of the bands $\Gamma_{2'}$ and Γ_{15}. This means that the Γ-X mixing for the ground states in Al-doped dot is suppressed. The Γ-X mixing of the singlet state is, of course, efficient. However, the singlet state, being an excited state, does not participate, in fact, in the PL. Therefore, it is not worth to expect an improvement of light emission in silicon NCs in consequence of their doping with aluminum.

Thus, summarizing our consideration, one can conclude that the choice of phosphorus as a dopant was not arbitrary. This impurity provides an efficient Γ-X mixing caused by the short-range Coulomb field. Such a mixing is strongly intensified by the quantum confinement of the NC, which leads to the considerable acceleration of radiative electron-hole transitions.

ACKNOWLEDGMENTS

The useful discussions with I. N. Yassievich are greatly appreciated. The authors thank the "Dynasty" Foundation (Russia) and the Russian Ministry of Education for financial support through Project No. RNP 2.1.1.2363.

[1] M. S. Hybertsen, Phys. Rev. Lett. **72**, 1514 (1994).
[2] C. Delerue, G. Allan, and M. Lannoo, Phys. Rev. B **64**, 193402 (2001).
[3] A. S. Moskalenko, J. Berakdar, A. A. Prokofiev, and I. N. Yassievich, Phys. Rev. B **76**, 085427 (2007).
[4] V. A. Belyakov, V. A. Burdov, R. Lockwood, and A. Meldrum, Adv. Opt. Technol. **2008**, 279502.
[5] M. Sykora, L. Mangolini, R. D. Schaller, U. Kortshagen, D. Jurbergs, and V. I. Klimov, Phys. Rev. Lett. **100**, 067401 (2008).
[6] I. Mihalcescu, J. C. Vial, A. Bsiesy, F. Muller, R. Romestain, E. Martin, C. Delerue, M. Lannoo, and G. Allan, Phys. Rev. B **51**, 17605 (1995).
[7] M. Lannoo, C. Delerue, and G. Allan, J. Lumin. **70**, 170 (1996).
[8] C. Delerue and M. Lannoo, *Nanostructures. Theory and Modelling* (Springer-Verlag, Berlin, 2004).
[9] Y. Kanemitsu, Phys. Rev. B **53**, 13515 (1996).
[10] J. Linnros, N. Lalic, A. Galeckas, and V. Grivickas, J. Appl. Phys. **86**, 6128 (1999).
[11] C. Garcia, B. Garrido, P. Pellegrino, R. Ferre, J. A. Moreno, J. R. Morante, L. Pavesi, and M. Gazzanelli, Appl. Phys. Lett. **82**, 1595 (2003).
[12] A. R. Wilkinson and R. G. Elliman, Phys. Rev. B **68**, 155302 (2003).
[13] M. Fujii, D. Kovalev, B. Goller, S. Minobe, S. Hayashi, and V. Y. Timoshenko, Phys. Rev. B **72**, 165321 (2005).
[14] S. Miura, T. Nakamura, M. Fujii, M. Inui, and S. Hayashi, Phys. Rev. B **73**, 245333 (2006).
[15] W. L. Wilson, P. F. Szajowski, and L. E. Brus, Science **262**, 1242 (1993).
[16] J. C. Vial, A. Bsiesy, F. Gaspard, R. Herino, M. Ligeon, F. Muller, R. Romestain, and R. M. Macfarlane, Phys. Rev. B **45**, 14171 (1992).
[17] D. I. Tetelbaum, I. A. Karpovich, M. V. Stepikhova, V. G. Shengurov, K. A. Markov, and O. N. Gorshkov, Surf. Invest. X-Ray Synchrotron Neutron Tech. **14**, 601 (1998).
[18] M. Fujii, A. Mimura, S. Hayashi, and K. Yamamoto, Appl. Phys. Lett. **75**, 184 (1999).
[19] A. Mimura, M. Fujii, S. Hayashi, D. Kovalev, and F. Koch, Phys. Rev. B **62**, 12625 (2000).
[20] D. I. Tetelbaum, S. A. Trushin, V. A. Burdov, A. I. Golovanov, D. G. Revin, and D. M. Gaponova, Nucl. Instrum. Methods Phys. Res. B **174**, 123 (2001).
[21] A. N. Mikhaylov, D. I. Tetelbaum, V. A. Burdov, O. N. Gorshkov, A. I. Belov, D. A. Kambarov, V. A. Belyakov, V. K. Vasiliev, A. I. Kovalev, and D. M. Gaponova, J. Nanosci. Nanotechnol. **8**, 780 (2008).
[22] F. Iori, E. Degoli, E. Luppi, R. Magri, I. Marri, G. Cantele, D. Ninno, F. Trani, and S. Ossicini, J. Lumin. **121**, 335 (2006).
[23] F. Iori, E. Degoli, R. Magri, I. Marri, G. Cantele, D. Ninno, F. Trani, O. Pulci, and S. Ossicini, Phys. Rev. B **76**, 085302 (2007).
[24] W. Kohn and J. M. Luttinger, Phys. Rev. **97**, 1721 (1955).
[25] S. T. Pantelides and C. T. Sah, Phys. Rev. B **10**, 621 (1974).
[26] J. P. Walter and M. L. Cohen, Phys. Rev. B **2**, 1821 (1970).
[27] H. Nara, J. Phys. Soc. Jpn. **20**, 778 (1965).
[28] V. A. Belyakov and V. A. Burdov, Phys. Rev. B **76**, 045335 (2007).
[29] D. V. Melnikov and J. R. Chelikowsky, Phys. Rev. Lett. **92**, 046802 (2004).
[30] Z. Zhou, M. L. Steigerwald, R. A. Friesner, L. Brus, and M. S. Hybertsen, Phys. Rev. B **71**, 245308 (2005).
[31] S. Ossicini, E. Degoli, F. Iori, E. Luppi, R. Magri, G. Cantele, F. Trani, and D. Ninno, Appl. Phys. Lett. **87**, 173120 (2005).
[32] Q. Xu, J. W. Luo, S. S. Li, J. B. Xia, J. Li, and S. H. Wei, Phys. Rev. B **75**, 235304 (2007).
[33] V. A. Belyakov and V. A. Burdov, Phys. Lett. A **367**, 128 (2007).
[34] L. E. Ramos, E. Degoli, G. Cantele, S. Ossicini, D. Ninno, J. Furthmuller, and F. Bechstedt, J. Phys.: Condens. Matter **19**, 466211 (2007).
[35] P. Y. Yu and M. Cardona, *Fundamentals of Semiconductors. Physics and Materials Properties* (Springer, New York, 2002).
[36] V. A. Burdov, Zh. Eksp. Teor. Fiz. **121**, 480 (2002) [JETP **94**, 411 (2002)].
[37] V. A. Belyakov and V. A. Burdov, J. Phys.: Condens. Matter **20**, 025213 (2008).
[38] O. J. Glembocki and F. H. Pollak, Phys. Rev. Lett. **48**, 413 (1982).
[39] O. J. Glembocki and F. H. Pollak, Phys. Rev. B **25**, 1193 (1982).
[40] A. Thranhardt, C. Ell, G. Khitrova, and H. M. Gibbs, Phys. Rev. B **65**, 035327 (2002).
[41] N. O. Lipari and A. Baldereschi, Solid State Commun. **25**, 665 (1978).
[42] G. A. Kachurin, S. G. Cherkova, V. A. Volodin, D. M. Marin, D. I. Tetelbaum, and H. Becker, Semiconductors **40**, 72 (2006).